

On the Use of Different Types of Standardized Dogbone Specimens for Tensile Tests of PLA Printed by MEX: A Comparative Analysis

Vasile Cojocaru

Lect. Dr. Eng.
Department of Engineering Science
Babeş-Bolyai University
Traian Vuia Sq. 1–4, 320085 Reşiţa
Romania

Doina Frunzaverde

Prof. Dr. Eng.
Department of Engineering Science
Babeş-Bolyai University
Traian Vuia Sq. 1–4, 320085 Reşiţa
Romania

Gabriela Marginean

Dipl-Eng, Dr. rer.nat.
Institute of Mechanical Engineering
Westphalian University of Applied Sciences
Neidenburger str. 43, 45897 Gelsenkirchen
Germany

The mechanical properties of 3D-printed parts produced by material extrusion (MEX) have been extensively investigated in recent years. However, there are no standards defining the test conditions and specimens' geometry, specifically for the parts obtained by this technology. The dogbone specimens, as defined by ISO 527-2 and ASTM D638, are mainly used for tensile tests of 3D printed polymers. This study presents a comparative analysis of four types of dogbone specimens made from polylactic acid (PLA) by material extrusion. Experimental results showed only slight variations (up to 2,34%) in the ultimate tensile strength (UTS) across the different types of specimens. On the other hand, they revealed the occurrence of failure at the boundary of the gauged section of the specimens, caused by a stress concentration in this area (as shown by numerical simulations) combined with irregularities and voids generated by the 3D printing strategy.

Keywords: material extrusion (MEX), fused deposition modelling (FDM), tensile tests, dogbone specimen, ultimate tensile strength (UTS), polylactic acid (PLA)

1. INTRODUCTION

The recent advancements in additive manufacturing (AM) technologies have facilitated their widespread application in complex domains such as aerospace engineering, electronics, energy systems, medical devices etc. [1-6].

The material extrusion (MEX) is a widely utilized AM process, particularly for thermoplastic polymers and composites materials, due to its ease of use and cost-effectiveness. In the MEX 3D-printing the material (typically in the form of a filament spool) is heated to a semi-liquid or molten state and then extruded through a nozzle to build up the parts, layer by layer, based on a digital model [7]. The material extrusion 3D-printing is commonly referred to as Fused Deposition Modelling (FDM) or Fused Filament Fabrication (FFF).

The mechanical behaviour of 3D printed MEX parts has been extensively studied in recent years [8-10]. Determining the optimal combination of process parameters that enhances the mechanical properties of MEX-printed polymers is crucial for utilizing this technique in the manufacturing of components for functional mechanical systems. The mechanical properties in tensile, compression, bending are influenced by several factors: the material and the pre-process treatments, the 3D printer type, the process parameters, the printing strategy, the post-process treatments [11-13].

Up to date, there is no dedicated standard to define the specimen geometry for tensile tests of the MEX 3D-printed parts. Broadly, the dogbone geometries as defined in ASTM D638 [14] and ISO 527-2 [15] (standards dedicated to tensile testing of plastics) have been used in previous research [11]. The dogbone specimens have a narrow calibrated central area (gauged section) and two wider end areas for gripping into the clamping grips. The transition between these areas is done by a fillet radius.

The MEX 3D-printing processes involve the deposition of a filament on a path defined by several process parameters. The printing strategy is correlated with the anisotropic behaviour of products [16-18] and with the internal geometrical particularities: voids, irregularities and stress concentrators in the regions with direction changes of the deposition path. These particularities, even though they do not influence the external shape of the part, can change its mechanical properties [19-21].

Analysing the printing strategy of a dogbone tensile specimen, it can be found that it is influenced by several process parameters, the most important being:

- the dimensions of the test specimen.
- the number of wall lines (contour lines).
- the infill pattern and the infill density.
- the raster angle and the orientation of the specimen on the build plate.
- the nozzle diameter and the layer height.
- the number of top/bottom layers and their geometrical particularities.

For example, Figure 1 presents the layer view of the ASTM D638 type II specimen printed under three distinct scenarios: two wall lines, five wall lines and seven wall lines (images generated by the Ultimaker

Received: February 2025, Accepted: April 2025
Correspondence to: Prof. Dr. Eng. Doina Frunzaverde
Department of Engineering Science, Babeş-Bolyai
University, Traian Vuia Sq. 1–4, 320085 Reşiţa,
Romania. E-mail: doina.frunzaverde@ubbcluj.ro
doi: 10.5937/fme2502326C

© Faculty of Mechanical Engineering, Belgrade. All rights reserved

FME Transactions (2025) 53, 335-343 **335**

Cura slicer software). It can be observed that the volume of material defined by the infill pattern decreases with increasing number of wall lines, reaching zero in the narrow area if seven wall lines are used.

Previous studies have identified several distinct scenarios in the tensile failure of MEX 3D-printed specimens [22, 23]:

- Inter-layers initiated failure, caused by weak adhesion of successive layers.
- In-layer initiated failure, caused by material voids or stress concentration in areas with change of the deposition path.
- Failure of the deposited filament.

It can be considered that the increase of wall lines number changes the failure mode of the specimen, reducing the influence of material voids, irregularities and stress concentrations [24].

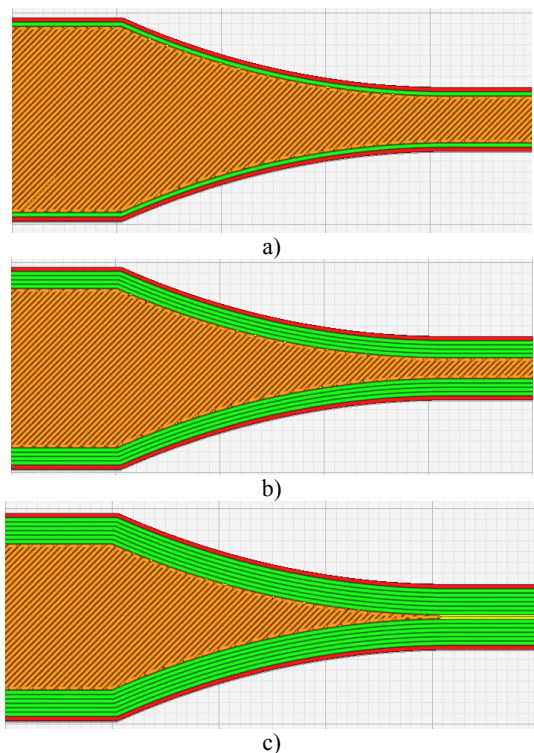


Figure 1. Layer view of ASTM D638 type II specimen fillet radius area with two wall lines (a), five wall lines (b), and seven wall lines (c)

The impact of the deposition path is more pronounced in the fillet radius area of the dogbone specimens. Figure 2 illustrates four filament deposition strategies: concentric, rectilinear, grid, and triangular infill patterns (with 100% infill density), generated by Ultimaker Cura for the ASTM D638 type II specimen. Voids, irregularities and stress concentrators are formed at the intersection of the infill patterns with the cylindrical surface (in the fillet radius region), that may lead to the occurrence of failure outside of the specimen's gauged section. The position of these voids depends on the infill pattern and density, but also on the other parameters presented above, in particular the specimen sizes and raster orientation.

The occurrence of failure in the fillet radius region of MEX 3D-printed specimens has been emphasized in many previous studies [22, 25-27].

Miller, Brown and Warner [27] performed a comparative analysis of ASTM D638 I, ASTM D638 IV dogbone specimens and ASTM D3039 (rectangular specimens with constant cross-section along the entire length, designed for composite materials). For each type, eight batches of specimens were printed, differentiated by raster orientation, layer resolution and infill density. The material used was ABS. The authors defined the test specimen failure performance as the ratio between the number of specimens with failure in the gauged section and the total number of specimens tested. The lowest values obtained for this parameter reached 20% for dogbone specimens (one of five specimens broke in the gauged section) and 80% for ASTM D3039 rectangular specimens. There were also differences in the values obtained for the ultimate tensile strength (UTS), the highest values being obtained for ASTM D638 IV specimens and the lowest for ASTM D3039 specimens, for all the cases analysed.

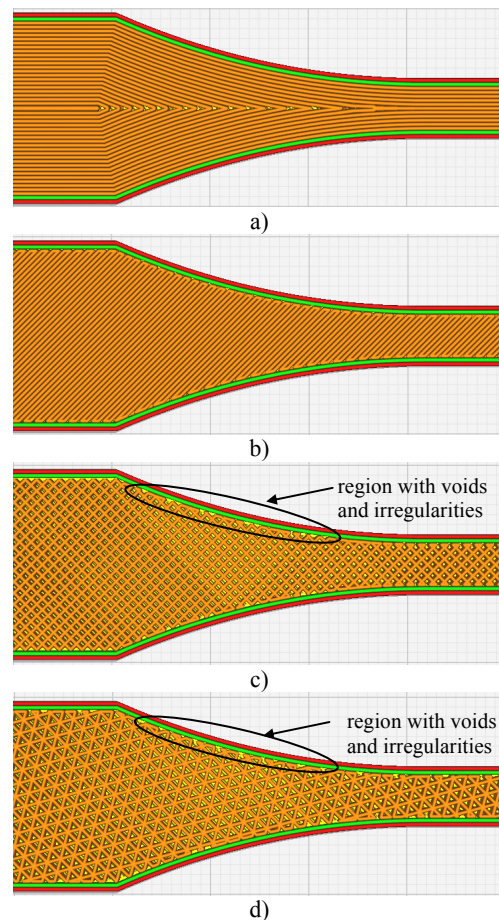


Figure 2. Layer view of ASTM D638 type II specimen fillet radius area with concentric (a), lines (b), grid (c) and triangles (d) infill patterns

Neivock et al. [28] analysed twelve types of tensile specimens: ASTM D638 I, ASTM D638 II, ASTM D638 III, ASTM D638 IV, ISO 527-2 1A, ISO 527-2 1B dogbone specimens for plastics and ASTM D3039 (constant cross-section), ISO 37 1, ISO 37 1A, ISO 37 2 specimens for composites. All the specimens were printed from PLA. The authors considered the coefficients of variation of the UTS, yield strength and modulus of elasticity, as well as the number of specimens broken outside the gauged section. It was

shown that the ISO 527-2 dogbone specimens exhibited the highest coefficient of variation of the results and the highest number of specimens broken outside the gauged section. In the analysis of the results, it should be noted that all specimens were printed using a low density (20%) honeycomb infill.

Faidallah et al. [25] conducted an analysis of ASTM D638 I, ISO 527-2 1A and ASTM 3039 (with tab bevel angle of 0°, 15° and 90°) specimens. All the specimens were printed from PET-G, using both flat and on-edge build orientations. The type of infill and the number of wall lines are not specified. Significant variations were observed in the ultimate tensile strength (UTS) values across the five specimen types, with the ISO 527-2 1A specimens exhibiting the lowest UTS values. These differences became more pronounced when the specimens were printed in the on-edge orientation. The authors did not specify whether a support structure was used for the on-edge printed dogbone specimens.

It is assumed that if a support structure is used for dogbone specimens (Fig. 3, exemplification made in Ultimaker Cura slicer software for an ISO 527-2 1A specimen disposed on edge), removal of the support leads to a surface with irregularities that may contribute to premature failure.

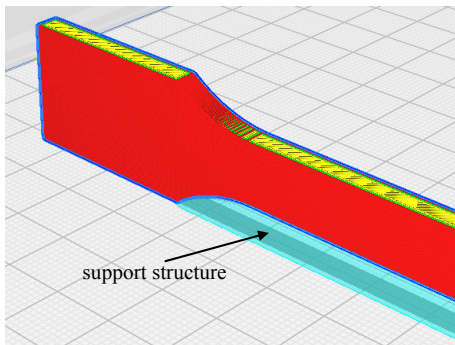


Figure 3. ISO 527-2 1A specimen (partial view) disposed on edge, using support structure (highlighted in cyan)

Ozen et al. [29] have shown that the deposition strategy (slicing mode) used in MEX printing significantly influences the mechanical properties of the material. The authors also indicated that local modifications of standardized specimens can reduce the risk of improper failure (ASTM D3039 specimens, ISO527-2 1A specimens and ISO527-2 1A specimens with increased width in the grips area were tested).

Frolich et al. [30] analysed the tensile behaviour of ISO 527-2 1A specimens manufactured in two scenarios: a) 3D printed of standard dogbone geometry, and b) cutting of standard dogbone geometry (using laser cutting, milling or water jet cutting) from a 3D printed rectangular plate. The authors emphasize that the cut-out specimens do not show notches in the fillet radius area, and the validity of the results increases for these specimens.

Sadaghian et al. [23] investigated the size effect of printed parts on the mechanical properties under tensile, compression, and bending conditions. ASTM D638 type II specimens, scaled between 0.5X and 2.5X of the standard dimensions, were used for tensile testing. For materials exhibiting brittle failure (polycarbonate

acrylonitrile butadiene styrene PC/ABS, acrylonitrile styrene acrylate ASA, and polylactic acid PLA), it was observed that the ultimate tensile strength (UTS) decreases significantly as the specimen size increases, with a reduction of approximately 33% for PLA.

The size effect can be linked to the number of parts printed simultaneously, as increasing the quantity of parts placed on the same build plate leads to the increase of deposition time between two successive layers [31].

Elmrabet and Siegkas [32] pointed out that dimensional variations in a part can cause differences in mechanical properties between large and small sized areas.

The use of dogbone specimens with increased thickness (10 mm in [33]) did not lead to the avoidance of problems related to the occurrence of failure in the region of fillet radius.

It follows from the above that the use of tensile specimens with different geometries makes it difficult to compare and generalize the conclusions obtained from tensile testing of FDM printed components. Comparative analyses on different specimen shapes are needed to finally contribute to the definition of a suitable specimen geometry for FDM printed polymers.

This study conducts a comparative analysis of the tensile behaviour of four types of dogbone specimens, as defined by ASTM D638 and ISO 527-2 standards, manufactured from PLA, using material extrusion. All specimens were produced with 100% infill density and the same process parameters. To further investigate the failure mechanism leading breakage at the fillet radius of specimens, a numerical analysis of the stress distribution was performed. Comparative analysis of dogbone specimens printed by MEX from PLA, using 100% infill, has not been found in previous research.

2. MATERIALS AND METHODS

The dogbone specimens analysed in this paper, defined by ISO 527-2 and ASTM D638 standards, are widely used in the tensile behaviour analysis of MEX 3D printed PLA. The main dimensional characteristics of the four types of specimens are shown in Table 1 (notations have been adopted according to ISO 527-2).

Table 1. The main dimensions of tensile specimens used in this research

Standard	ISO 527-2	ASTM D638		
		I	II	IV
Specimen type	1A	I	II	IV
Thickness, h [mm]	4	2.6	3.2	3.2
Width of narrow section (gauged section), b_1 [mm]	10	13	6	6
Length of narrow section (gauged section), l_1 [mm]	80	57	57	33
Fillet Radius, r [mm]	24	76	76	14
Width at ends, b_2 [mm]	20	19	19	19
Overall length, l_3 [mm]	170	165	183	115
Initial distance between grips, L [mm]	115	115	135	65

The 3D geometry of the samples was created by SolidWorks. The Ultimaker Cura slicer software was used to set the process parameters, to define the printing strategy and to generate the NC file for the printer.

2.1 Additive manufacturing of specimens

The test specimens were manufactured using an Ultimaker 2+ Connect printer, with the printing space fully enclosed. This FDM 3D printer has a maximum workspace of 223 x 220 x 205 mm³. For the nozzle with 0.4 mm diameter, the layer thicknesses can be set in the range of 0.02-0.2 mm. The positioning resolution is 12.5 μm (X axis and Y axis) and 5 μm (Z axis).

Ultimaker PLA filament (Silver Metallic colour) with a diameter of 2.85 mm was used. All specimens were made from the same spool of filament. Each specimen was printed individually (one specimen on the printing plate), centred, using YXZ – flat build orientation (the build orientation is defined according to ISO/ASTM 52921:2013 [34]).

The process parameters (Table 2) were maintained the same for all samples and were set at values selected according to the filament manufacturer's recommendations and considering previous research [35, 36]. 100% lines infill, with 45°/-45° raster (with respect to the XY axes) and two wall lines were used for all layers.

Table 2. The process parameters for 3D printing of specimens

Parameter	U.M.	Value
Layer thickness, t	mm	0.1
Printing head temperature, T _H	°C	210
Build plate temperature, T _B	°C	60
Printing speed, s _p	mm/s	50
Nozzle diameter, d _n	mm	0.40
Build orientation	-	YXZ
Raster angle, θ	-	45°/-45°
Number of wall lines, W _L (-)	-	2
Infill pattern	-	Lines
Infill density	%	100
Filament diameter, d _f	mm	2.85
Material	-	PLA

No pre-process or post-process treatments were applied; the specimens were kept at room temperature until the tensile tests.

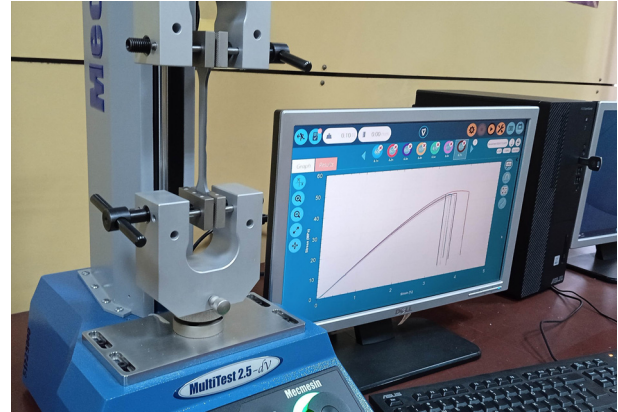
2.2 Tensile tests

The tensile tests were performed on a Mecmesin MultiTest 2.5 dV universal tensile equipment with a maximum capacity of 2500 N (figure 4a). The test equipment has a positioning resolution of 1 μm and the force cell ensures a measurement accuracy of ± 0.5% of the measured value. The Vector Pro MT software was used for the command, the control and the data acquisition. A working speed of 10 mm/min was used for all tests.

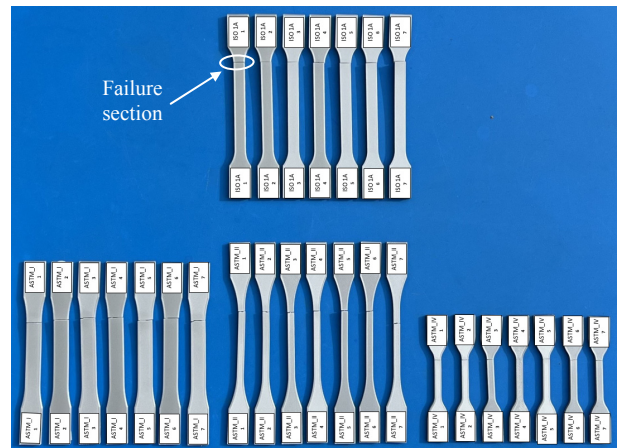
Seven tests were performed for each type of specimen, to check the reproducibility of the results.

Figure 4 b) shows the aspect of the specimens after tensile testing.

The tensile tests aimed to determine the ultimate tensile strength (UTS) and the stress-strain curve, as well as to analyse the failure mode of the specimens.



a)



b)

Figure 4. Tensile tests: a) Mecmesin MultiTest 2.5 dV universal tensile equipment with Vector Pro MT software, b) the aspect of the specimens after tensile testing

2.3 Finite element analysis

Numerical simulations were performed under static stress loading using SolidWorks Simulation, to analyse the stress distribution in the region of the specimen radius. The following data were defined in the simulation:

- blended curvature-based mesh (Figure 5), with the same maximum size of finite elements.
- one end of the specimen was considered fixed (on the surfaces in contact with the tensile grips).
- a static force F_i was applied at the other end of the specimen, on the surfaces in contact with the tensile grips. The force was calculated with the relation:

$$F_i = \sigma_{ref} \cdot A_i \quad (1)$$

where A_i is the cross-sectional area of the test specimen in the gauged section, and $\sigma_{ref} = 20 \text{ MPa}$ is a reference value of the stress in the gauged section (this value was arbitrarily chosen).

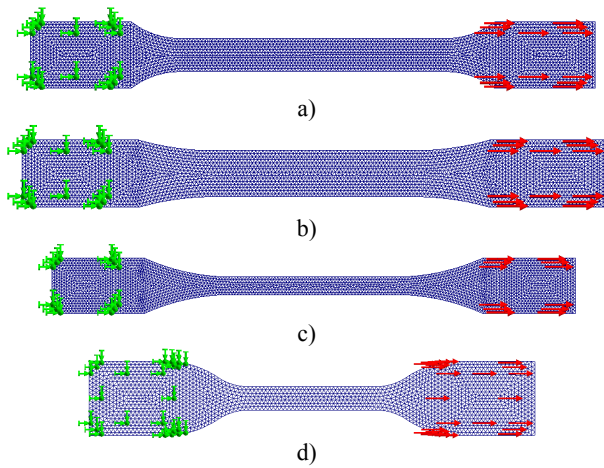


Figure 5. The mesh, the fixing conditions and the loadings applied in FEM studies, for the four types of specimens: a) ISO 527-2 1A, b) ASTM D638 type I, c) ASTM D638 type II, d) ASTM D638 type IV.

2.4 Structural analysis

The mezostructures of the tensile samples were investigated with the aid of a Leica MZ 7.5 stereomicroscope (Leica Microsystems, Wetzlar, Germany). For each type of specimens, images of the fractured sections were recorded at a magnification of 10x.

3. RESULTS AND DISCUSSION

The UTS values for all tested specimens are centralized in Table 3. From the seven values obtained for each type of specimen, the two values farthest from the mean have been eliminated (highlighted in italics). The UTS means calculated in this way are shown in Figure 6. The differences between the means are small. The minimum value of 51.53 MPa was obtained for the ISO 527-2 type 1A specimen, while the maximum value of 52.73 MPa was obtained for the ASTM D638 type II specimen (these values correspond to a variation of 2.34%). The highest standard deviation was found for the ASTM D638 type IV specimen, and the lowest standard deviation was found for the ISO 527-2 type 1A specimen.

Table 3. Ultimate tensile strength values for all specimens

UTS [MPa]						
ISO 527-2, type 1A specimens						
I_I1	I_I2	I_I3	I_I4	I_I5	I_I6	I_I7
51.71	51.04	<i>51.57</i>	51.35	51.67	51.33	<i>50.74</i>
ASTM D638, type I specimens						
A_I1	A_I2	A_I3	A_I4	A_I5	A_I6	A_I7
<i>50.12</i>	52.12	51.38	52.29	<i>50.96</i>	52.65	52.71
ASTM D638, type II specimens						
A_II1	A_II2	A_II3	A_II4	A_II5	A_II6	A_III7
53.59	53.03	<i>49.10</i>	52.32	52.11	52.60	<i>41.55</i>
ASTM D638, type IV specimens						
A_IV1	A_IV2	A_IV3	A_IV4	A_IV5	A_IV6	A_IV7
52.76	53.31	50.98	<i>51.28</i>	51.09	51.29	<i>50.84</i>

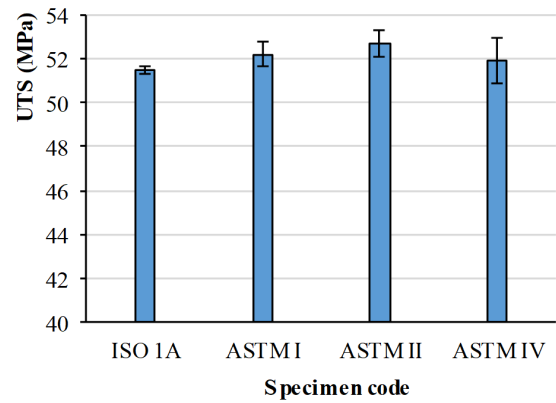


Figure 6. The variation of the UTS means

The Figures 7-10 show the stress (σ) – strain (ϵ) curves for the four types of specimens, and the Table 4 presents the average values for the slope of the curve ($tg(\alpha) = \sigma \cdot \epsilon^{-1}$) in the domain of proportionality. It can be noticed that $tg(\alpha)$ has the maximum value for the ASTM638 type II specimens.

Starting from the definition of the axial stress for tensile loading and from the Hooke's law, the next equation can be written:

$$\sigma \cdot \epsilon^{-1} = (F \cdot \Delta l^{-1}) \cdot (l_1 \cdot A^{-1}) \quad (2)$$

where: F – the applied force, Δl – the elongation, l_1 – the length of gauged section, A – the cross-sectional area in the gauged section of the specimen.

The values of the $l_1 \cdot A^{-1}$ ratio are summarized in Table 4. It can be noticed that the highest value of $tg(\alpha)$ corresponds to the largest $l_1 \cdot A^{-1}$ ratio.

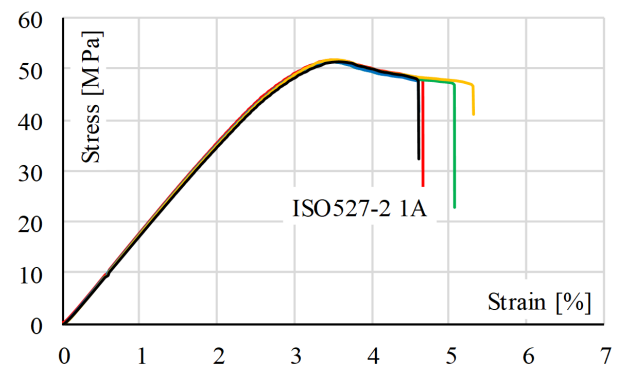


Figure 7. The stress – strain curves for ISO 527-2 1A specimens

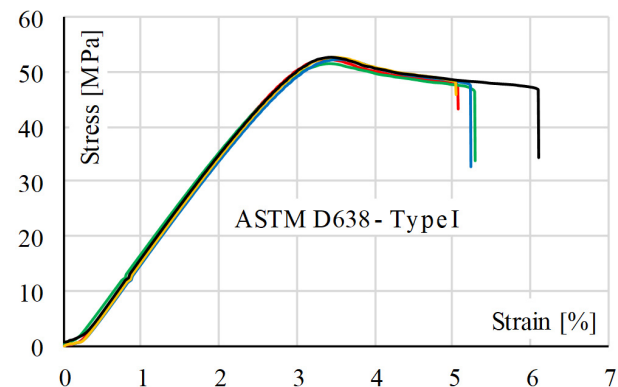


Figure 8. The stress – strain curves for ASTM D638 type I specimens

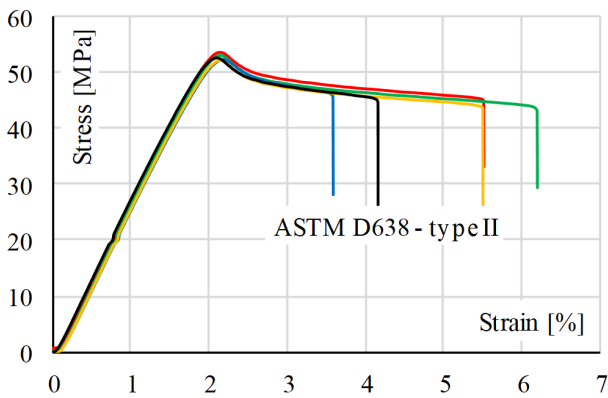


Figure 9. The stress – strain curves for ASTM D638 type II specimens

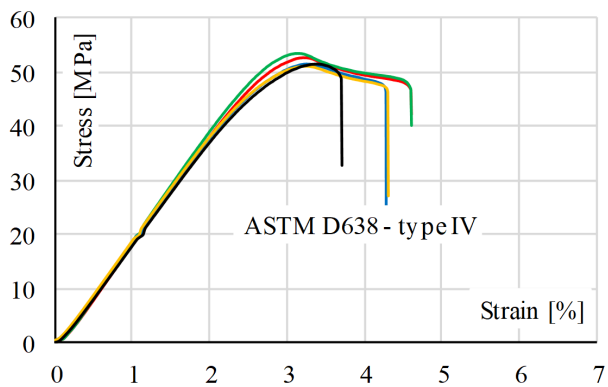


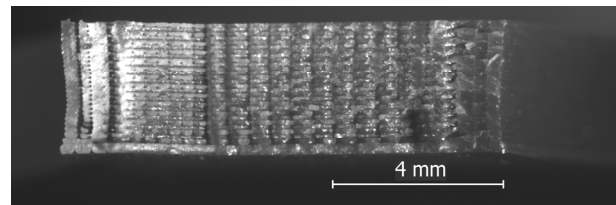
Figure 10. The stress – strain curves for ASTM D638 type IV specimens

Table 4. The slope of stress-strain curves correlated to the dimensions of gauged section of the specimens

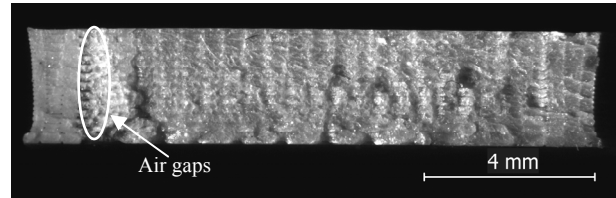
Standard	ISO 527-2	ASTM D638		
	1A	I	II	IV
Specimen type	1A	I	II	IV
$tg(\alpha)$	18.328	17.882	29.201	20.305
h [mm]	4	2.6	3.2	3.2
b_1 [mm]	10	13	6	6
l_1 [mm]	80	57	57	33
$A=b \cdot h$ [mm ²]	40	33.8	19.2	19.2
$l_1 \cdot A^{-1}$ [mm ⁻¹]	2	1.68	2.96	1.71

In terms of repeatability of results for a batch of specimens, the standard deviations are relatively small (Figure 6). The curves show good overlapping in the elastic domain. The discrepancies are observed mainly for the strain-at-break values.

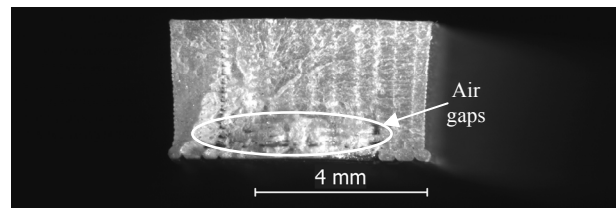
Previous research [11, 35] revealed that the printing temperature is an important influential parameter in respect of the prints' mezostructure and thereby its UTS values. Considering that the thermal printing conditions are dependent on the dimensions of the printed part [31], it was to be expected that samples with different geometries and dimensions might have different structures, in terms of adhesion between successive layers and/or adjacent roads. Therefore, the cross-section of the specimens after tensile testing was examined by light microscopy. Representative images are presented in Figure 11.



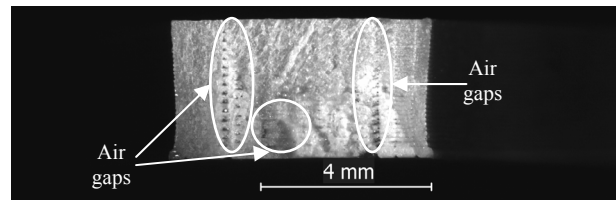
a)



b)



c)



d)

Figure 11. The cross-section of the specimens after the tensile testing: a) ISO 527-2 1A, b) ASTM D638 type I, c) ASTM D638 type II, d) ASTM D638 type IV. Stereomicroscopic captures

As one may observe in Figure 11, the most compact mezostructure resulted in case of the ASTM D638 type II specimen, which obtained the highest UTS value. In the case of the specimens ASTM D638 type I and especially ASTM D638 type IV air gaps are clearly visible in the peripheral areas, while in case of the ISO 527-2 1A sample air gaps may be observed throughout the whole section, with specific appearance of under-extrusion. This phenomenon might manifest itself even more accentuated in case of other colored PLA filaments, as shown in [31].

Figure 4 shows that for most of the tested specimens the failure occurred at the limits of the gauged section. Looking to explain this, FEM simulations were conducted.

For all specimens, the loading conditions were configured to ensure a stress of 20 MPa in the gauged section. Figures 12-15 illustrate the charts of von Mises stress distribution, highlighting the stress increase in the region of fillet radius. The stress concentration factor in this region was calculated using the following equation:

$$c_i = \sigma_{max} \cdot \sigma_{ref}^{-1} \quad (3)$$

where: σ_{max} – the maximum value of von Mises stress in the region of the fillet radius, $\sigma_{ref}=20$ MPa the reference value of von Mises stress in the gauged section.

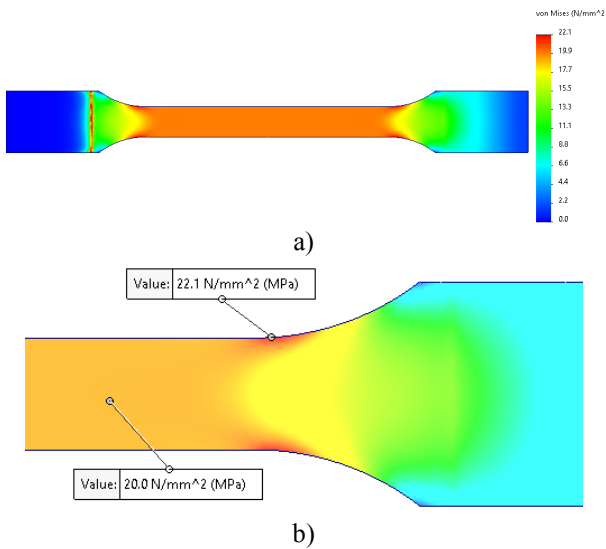


Figure 12. The chart of von Mises stress for ISO 527-2 1A specimens. General view (a) and detail (b)

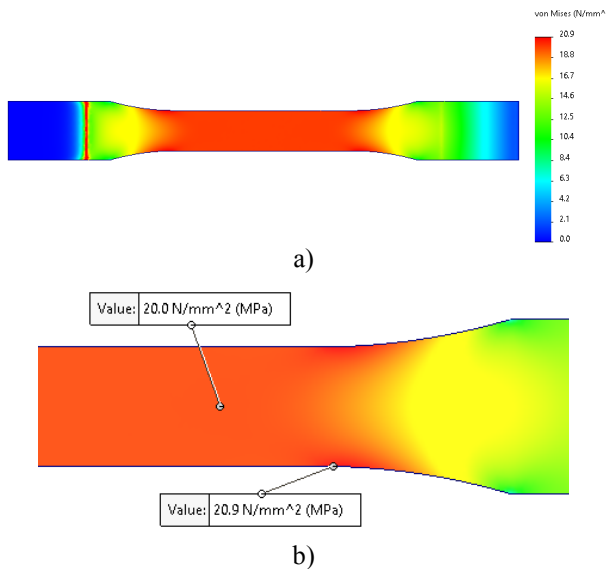


Figure 13. The chart of von Mises stress for ASTM D638 type I specimens. General view (a) and detail (b)

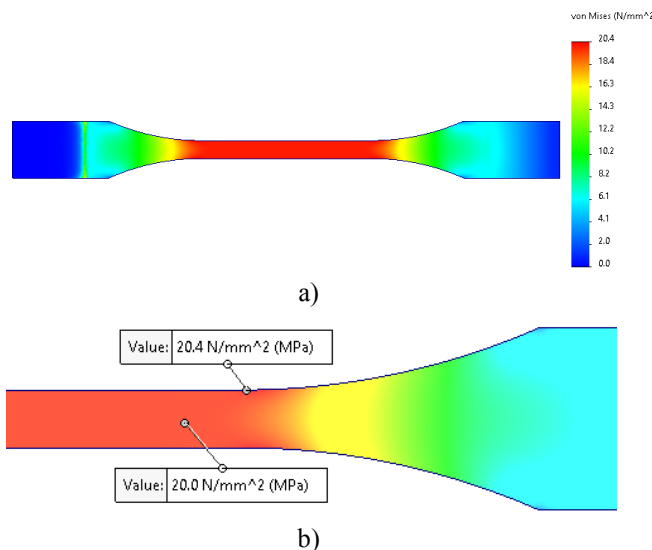


Figure 14. The chart of von Mises stress for ASTM D638 type II specimens. General view (a) and detail (b)

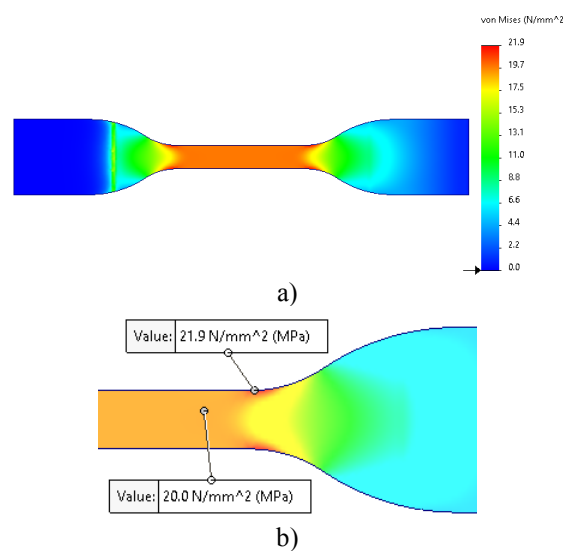


Figure 15. The chart of von Mises stress for ASTM D638 type IV specimens. General view (a) and detail (b)

The maximum value of the stress-concentration factor was obtained for the ISO 527-2 1A specimen ($c=1.105$) and the minimum value for the ASTM D638 type II specimen ($c=1.02$). It can be observed that the stress gradients are not large, but given the irregularities and voids in the material, generated by the filament deposition strategy, these gradients may cause the occurrence of failure outside the gauged section.

The use of the specimens with a constant cross-section (without a fillet radius) can minimize or even eliminate the irregularities generated by the 3D printing deposition strategy, as these irregularities are accentuated by the change in the specimen width. However, in case of specimens with a constant cross-section for the entire length, the failure might occur anywhere, including the area of the clamping grips.

Although the differences in the mean UTS values obtained for the four specimen types are relatively small (maximum of 2.34%), the occurrence of failure at the boundary of the gauged area constitutes a nonconformity. Therefore, it is critical to establish a standard that defines the optimal conditions and specimen geometry for tensile testing of MEX 3D-printed polymeric materials.

4. CONCLUSION

The experimental and the numerical analysis of the tensile behaviour of four types of dogbone specimens, 3D printed from PLA, led to the following conclusions:

- The differences between the mean values of ultimate tensile strength for the four types of dogbone specimens are small (up to 2.34%). These values are much lower than those presented in the literature for other polymeric materials (PET-G) or for the same material (PLA), but printed using low infill densities.
- Significant differences in the slope of the stress-strain curves occur between the four types of dogbone specimens. The higher slope corresponds to ASTM D638, type II specimens.

- The printing strategy used in material extrusion can lead to irregularities in the area of the fillet radius of dogbone specimens.
- For most of the specimens, failure occurs at the limits of the gauged section. This can be caused by the effect of irregularities induced by the printing strategy, cumulated with the effect of stress concentrators from the area of the fillet radius (revealed by numerical simulations).

REFERENCES

- [1] Ngo, T.D., Kashani, A., Imbalzano, G., Nguyen, K.T.Q and Hui, D.: Additive manufacturing (3D printing): A review of materials, methods, applications and challenges, *Composites Part B: Engineering*, Vol. 143, pp. 172-196, 2018.
- [2] Sun, C., Wang, Y., McMurtrey, M., Jerred, N., Liou, F. and Li, J.: Additive manufacturing for energy: A review, *Applied Energy*, Vol. 282, Part A, 116041, 2021.
- [3] Kumar, R., Kumar, M. and Chohan, J. S.: The role of additive manufacturing for biomedical applications: A critical review, *Journal of Manufacturing Processes*, Vol. 64, pp. 828–850, 2021.
- [4] Bhatia, A. and Sehgal, A. K.: Additive manufacturing materials, methods and applications: A review, *Materials Today: Proceedings*, Vol. 81, pp. 1060-1067, 2023.
- [5] Pavlovic, A., Sljivic, M., Krajsnik, M., Ilic, J. and Anic, J.: Polymers in Additive Manufacturing: The Case of a Water Pump Impeller, *FME Transaction*, Vol. 45, No. 3, pp. 354–359, 2017.
- [6] Nedelcu, D., Cojocaru, V., Micu, L.M., Florea, D. and Hluscu, M.: Using of Polymers for Rapid Prototyping of an Axial Microturbine Runner and Wicked Gates, *Materiale Plastice*, Vol. 56, No. 2, pp. 454-459, 2019.
- [7] Goh, G.D., Yap, Y.L., Tan, H.K.J., Sing, S.L., Goh, G.L. and Yeong, W.Y.: Process-Structure-Properties in Polymer Additive Manufacturing via Material Extrusion: A Review, *Crit. Rev. Solid State Mat. Sci.*, Volume 45, No. 2, pp. 113 – 133, 2020.
- [8] Popescu, D., Zapciu, A., Amza, C., Baci, F. and Marinescu, R.: FDM process parameters influence over the mechanical properties of polymer specimens: A review, *Polym. Test*, Vol. 69, pp. 157 – 166, 2018.
- [9] Harris, M., Potgieter, J., Archer, R. and Arif, K.M.: Effect of Material and Process Specific Factors on the Strength of Printed Parts in Fused Filament Fabrication: A Review of Recent Developments, *Materials*, Vol. 12, Art. 1664, 2019.
- [10] Gordelier, T.J., Thies, P.R., Turner, L. and Johanning, L.: Optimising the FDM additive manufacturing process to achieve maximum tensile strength: a state-of-the-art review, *Rapid Prototyping J.*, Vol. 25, No. 6, pp. 953 – 971, 2019.
- [11] Cojocaru, V., Frunzaverde, D., Miclosina, C.-O. and Marginean, G.: The influence of the process parameters on the mechanical properties of PLA specimens produced by fused filament fabrication—A review, *Polymers*, Vol. 14, No. 5, Art. 886, 2022.
- [12] Sljivic, M., Pavlovic, A., Ilic, J., Stanojevic, M. and Todorovic, S.: Comparing the Accuracy of Professional and Consumer Grade 3D Printers in Complex Models Production, *FME Transaction* 2017, Vol. 45, No. 3, pp. 348–353, 2017.
- [13] Zhang, P., Wang, Z., Li, J., Li, X. and Cheng, L.: From materials to devices using fused deposition modeling: A state-of-art review, *Nanotechnology Reviews*, Vol. 9, No. 1, pp. 1594-1609, 2020.
- [14] ASTM International. ASTM D638-14; Standard Test Method for Tensile Properties of Plastics. ASTM International: West Conshohocken, PA, USA, 2014.
- [15] International Organization for Standardization. ISO 527-2:2012; Plastics—Determination of Tensile Properties—Part 2: Test Conditions for Molding and Extrusion Plastics. International Organization for Standardization: Geneva, Switzerland, 2012.
- [16] Lin, X., Wu, S., Wang, D., Gong, M., Zhang, L., Liu, Y., Zhang, L., Lu, Y. and Wang, R.: Super elastic-plastic behavior of the surface grooves resulting in tensile anisotropy of 3D-printed elastomers, *Additive Manufacturing*, Vol. 82, 104030, 2024.
- [17] Bembenek, M., Kowalski, L. and Kosoń-Schab, A.: Research on the Influence of Processing Parameters on the Specific Tensile Strength of FDM Additive Manufactured PET-G and PLA Materials, *Polymers* Vol. 14, No. 12, Art. 2446, 2022.
- [18] Cojocaru, V., Frunzaverde, D. and Miclosina, C.O.: On the Behavior of Honeycomb, Grid and Triangular PLA Structures under Symmetric and Asymmetric Bending, *Micromachines*, vol. 14, No. 1, Art. 120, 2023.
- [19] Abouel Nour, Y. and Gupta, N.: Assisted defect detection by in-process monitoring of additive manufacturing using optical imaging and infrared thermography, *Additive Manufacturing*, Vol. 67, 103483, 2023.
- [20] Abouel Nour, Y., Rakauskas, N., Naquila, G. and Gupta, N.: Tensile testing data of additive manufactured ASTM D638 standard specimens with embedded internal geometrical features, *Scientific Data*, Vol. 11, No. 1, 506, 2024.
- [21] Ng, F. L., Tran, T. Q. and Liu, T.: A methodology to develop part acceptance criteria model using non-destructive inspection technique for FDM printed part, *Materials Today: Proceedings*, Vol. 70, pp. 310–316, 2022.
- [22] Yao, T., Deng, Z., Zhang, K. and Li, S.: A method to predict the ultimate tensile strength of 3D printing polylactic acid (PLA) materials with different printing orientations, *Composites Part B: Engineering*, Vol. 163, pp. 393–402, 2019.

- [23] Sadaghian, H., Dadmand, B., Pourbaba, M., Jabbari, S. and Yeon, J.H.: The Effect of Size on the Mechanical Properties of 3D-Printed Polymers, *Sustainability*, Vol. 16, No. 1, Art. 356, 2024.
- [24] Hamzah, A.H., Paijan, L.H., Abu Bakar, M.H., Mamat, M.F., Maidin, N.A. and Musa, S.I.: Effect of Wall Line Count on the Mechanical Properties of FDM 3D-Printed PLA Parts, *Malaysian Journal of Microscopy*, Vol. 20, No. 2, pp. 34-44, 2024.
- [25] Faidallah, R. F., Hanon, M. M., Vashist, V., Habib, A., Szakál, Z. and Oldal, I.: Effect of Different Standard Geometry Shapes on the Tensile Properties of 3D-Printed Polymer, *Polymers*, Vol. 15, No. 14, Art. 3029, 2023.
- [26] Yao, T., Ye, J., Deng, Z., Zhang, K., Ma, Y. and Ouyang, H.: Tensile failure strength and separation angle of FDM 3D printing PLA material: Experimental and theoretical analyses, *Composites Part B: Engineering*, Vol. 188, 107894, 2020.
- [27] Miller, A., Brown, C. and Warner, G.: Guidance on the Use of Existing ASTM Polymer Testing Standards for ABS Parts Fabricated Using FFF, *Smart and Sustainable Manufacturing Systems*, Vol. 3, no. 1, 122-38, 2019.
- [28] Neivock, M., Gomide, C., Nogueira, V., Caires A. and Oliveira S.: Comparative analysis of specimen geometries in material extrusion 3D printing: Implications for mechanical property evaluation, *Journal of Applied Polymer Science*, Vol. 141, no. 6, e54991, 2023.
- [29] Özen, A., Auhl, D., Völlmecke, C., Kiendl, J. and Abali, B.E.: Optimization of Manufacturing Parameters and Tensile Specimen Geometry for Fused Deposition Modeling (FDM) 3D-Printed PETG, *Materials*, Vol. 14, No. 10, Art. 2556, 2021.
- [30] Frölich, F., Bechtloff, L., Scheuring, B. M., Heuer, A. L., Wittemann, F., Kärger, L. and Liebig, W. V.: Evaluation of Mechanical Properties Characterization of Additively Manufactured Components, *Prog. Addit. Manuf.*, 2024.
- [31] Cojocaru, V., Turiac, R.R., Frunzaverde, D., Trisca, G., Bacescu, N. and Marginean, G.: Effect of the Printing Scenario on the Dimensional Accuracy and the Tensile Strength of Different Colored PLA Specimens Produced by Fused Deposition Modeling, *Appl. Sci.*, Vol. 14, No. 17, Art. 7642, 2024.
- [32] Elmrabet, N., Siegkas, P.: Dimensional considerations on the mechanical properties of 3D printed polymer parts, *Polymer Testing*, Vol. 20, 106656, 2020.
- [33] Mazen, A., McClanahan, B. and Weaver, J.M.: Factors affecting ultimate tensile strength and impact toughness of 3D printed parts using fractional factorial design, *Int J Adv Manuf Technol*, Vol. 119, pp. 2639–2651, 2022.
- [34] ISO/ASTM 52921:2013; Standard Terminology for Additive Manufacturing—Coordinate Systems and Test Methodologies. International Organization for Standardization: Geneva, Switzerland, 2013.
- [35] Frunzaverde, D., Cojocaru, V., Ciubotariu, C.-R., Miclosina, C.-O., Ardeljan, D.D., Ignat, E.F. and Marginean, G.: The Influence of the Printing Temperature and the Filament Color on the Dimensional Accuracy, Tensile Strength, and Friction Performance of FFF-Printed PLA Specimens, *Polymers*, Vol. 14, No.10, Art. 1978, 2022.
- [36] Frunzaverde, D., Cojocaru, V., Bacescu, N., Ciubotariu, C.-R., Miclosina, C.-O., Turiac, R.R. and Marginean, G.: The Influence of the Layer Height and the Filament Color on the Dimensional Accuracy and the Tensile Strength of FDM-Printed PLA Specimens, *Polymers*, Vol. 15, No. 10, Art. 2377, 2023.

**О УПОТРЕБИ РАЗЛИЧИТИХ ВРСТА
СТАНДАРДИЗОВАНИХ УЗОРАКА „ПСЕЋЕ
КОСТИ“ ЗА ИСПИТИВАЊА ЗАТЕЗАЊА PLA
ШТАМПЕНИХ ПОМОЋУ МЕХ-А: УПОРЕДНА
АНАЛИЗА**

В. Којокару, Д. Фрунзаверде, Г. Маргинеан

Механичка својства 3Д штампаних делова произведених екструзијом материјала (МЕХ) су опширно истраживана последњих година. Међутим, не постоје стандарди који дефинишу услове испитивања и геометрију узорака, посебно за делове добијене овом технологијом. Узорци „псеће кости“, како је дефинисано ISO 527-2 и ASTM D638, углавном се користе за испитивања затезања 3Д штампаних примера. Ова студија представља упоредну анализу четири типа узорака „псеће кости“ направљених од полилактичне киселине (PLA) екструзијом материјала. Експериментални резултати показали су само мале варијације (до 2,34%) у граничној затезној чврстоћи (UTS) код различитих типова узорака. С друге стране, открили су појаву квара на граници мерног пресека узорака, узрокованог концентрацијом напона у овој области (као што је показано нумеричким симулацијама) у комбинацији са неправилностима и шупљинама генерисаним 3Д стратегијом штампања.

